CFSRC COLLOQUIUM

Proceedings of the Cold-Formed Steel Research Consortium Colloquium
20-22 October, 2020 (cfsrc.org)

Modeling of stress-strain relationship of advanced high-strength cold-formed steel at elevated temperature

Yu Xia[1], Xia Yan[2], Thomas Gernay[3], Hannah B. Blum[4]

Abstract
Recent material advances in the steel manufacturing processes have led to materials with greatly enhanced capabilities at competitive cost. New grades of cold-formed steels, referred to as Advanced High-Strength Steels (AHSS), have been developed with yield strengths up to 1200 MPa and ultimate strengths up to 1900 MPa. However, the behavior of these novel materials must be understood and characterized under extreme environments which may arise in structural applications, including high temperatures resulting from fire. In most current design codes, including the American Iron and Steel Institute standard, Eurocode and the Australian Standard, the properties of high strength cold-formed steel subjected to fire conditions are limited or non-existent. A series of steady-state coupon tensile tests for two families of AHSS with nominal yield strength of 340 MPa, 700 MPa, 1030 MPa and 1200 MPa at various uniform temperature stages from ambient to 700°C were carried out. A new constitutive model was proposed based on the characteristics of AHSS stress-strain curves from the tests, and a good agreement between the test data and the model was achieved. In addition, existing stress-strain models from previous studies were investigated to represent the material properties of AHSS at elevated temperatures and compared with the updated model. The fittings of the multiple material models for various families and grades of AHSS were evaluated. The data generated by this research addresses fire safety design and will be essential in supporting the adoption of these next generation steels in future infrastructure.

1. Introduction

Recent advances in steel manufacturing processes have led to materials with greatly enhanced capabilities at competitive cost. New grades of steel, referred to as Advanced High-Strength Steels (AHSS), have been recently developed with yield strengths up to 1200 MPa, ultimate strengths up to 1900 MPa, and tensile elongations of at least 10%. Currently, AHSS have been used in the automobile industry. The adoption of AHSS in the construction industry can provide many benefits, notably with cold-formed steel (CFS) structures which provide efficient, lightweight, and resilient solutions for a range of building applications. Nevertheless, the behavior of these novel materials must be understood and characterized under extreme environments which may arise in structural applications, including high temperatures resulting from fire. In the current design codes [1][2][3][4][5], the deterioration of essential mechanical properties at elevated temperature including elastic modulus and yield strength are recommended based on research on hot-rolled steels or conventional CFS. Research on the mechanical property deterioration of cold-formed high strength steel subjected to fire loads are extremely limited or non-existent. The yield strength and tensile strength of cold-formed steel members increase relative to that of the sheet due to the cold-forming process. However, these material property increases are quickly deteriorated when the steel is exposed to elevated temperatures. This phenomenon is even more severe on cold-formed high strength steels [6].

AHSS are produced by controlling the chemistry and cooling rate from the austenite phase or austenite plus ferrite phase. Research has provided chemical and processing combinations that have created multiple additional grades of AHSS and improved properties. AHSS are primarily steels with a multiphase microstructure containing one or more phases other than ferrite, pearlite, or cementite, which could include martensite, bainite, austenite, and/or retained austenite in quantities sufficient to produce unique mechanical properties [7]. Therefore, in order to thoroughly understand the mechanical properties of these novel materials at elevated temperature, well-designed experimental studies are important.

[1]Graduate Research Assistant, Department of Civil & Environmental Engineering, University of Wisconsin-Madison, yxia44@wisc.edu
[2]Graduate Research Assistant, Department of Civil and Systems Engineering, Johns Hopkins University, xyan18@jhu.edu
[3]Assistant Professor, Department of Civil and Systems Engineering, Johns Hopkins University, tgernay@jhu.edu
[4]Assistant Professor, Department of Civil & Environmental Engineering, University of Wisconsin-Madison, hannah.blum@wisc.edu

The tensile test in a steady-state manner is widely used to investigate steel constitutive relationship and mechanical properties at elevated temperature, which is also adopted in this study. During the steady-state tensile coupon test, the specimen is heated up to a target elevated temperature and that temperature is then held constant. Then tension load is applied on the specimen in a displacement control manner with constant loading rate until fracture of the specimen. The steady-state test produces the stress-strain relationship at the target temperature, which can be used directly for characterization of material properties.

The steady-state test method has been previously adopted in several studies on material properties at elevated temperature on CFS with both conventional and high strengths. Lee [8] conducted studies on CFS with yield strengths of 300 MPa, 500 MPa and 550 MPa with thickness ranging from 0.4 mm to 1.2 mm subjected to high temperature up to 800°C. They found the recommendations from standards were unconservative for their materials and new recommendations for yield strength and elastic modulus at elevated temperatures were proposed. Chen [9] investigated 1 mm thick G550 CFS subjected to high temperature up to 600°C by both steady-state and transient-state methods. Their comparison showed the BS5950 [3] provided safe prediction with steady-state result while other standards provided unconservative recommendations. They proposed a unified equation for the retention factors for elastic modulus, yield strength, and ultimate strength. Huang [10] conducted a series of experiments on lean duplex stainless CFS with ultimate strength of 830 MPa subjected to high temperature up to 900°C. They determined that the elongation and the ultimate strain could be predicted by Eurocode 3: Part 1-2 [4], while the elastic modulus and yield strength were unsafe based on the Standard's recommendation. An accurate modeling of stress-strain relationship is also important in structural and material simulation. Eurocode 3: Part 1-2 [4] provides an approximation of stress-strain relationship for carbon steel at elevated temperatures, while the critical strains, including yield strain, limiting strain for yield strength, and ultimate strain, are fixed values which may be inadequate for different types of steels. Lee [8]) and Chen [11] proposed models based on Ramberg-Osgood equations for specific steel families and their models were adopted and calibrated by many other researchers for their own steel types.

In this study, a series of tensile coupon tests to study the stress-strain behavior and material properties (including elastic modulus, yield strength and ultimate strength) of AHSS subjected to high temperature up to 700°C in steady-state manner was carried out. Pinned tensile coupon specimens were cut from four steel sheets with two different thicknesses and four different nominal yield strengths. The modeling of material stress-strain relationship is discussed. An updated two-stage plus linear model based on the Ramberg-Osgood equation was proposed and verified. The fittings of the test data using existing models for CFS at elevated temperature from previous studies were performed and compared with the newly proposed model.

Table 1: Basic information for AHSS sheets

Steel	t_n (mm)	σ_{yn} (MPa)	σ_{un} (MPa)	coating
DP-340	1.4	340	590	uncoated
DP-700	1.4	700	980	coated
MS-1030	1.0	1030	1300	uncoated
MS-1200	1.0	1200	1500	uncoated

Table 2: Typical chemical mass composition of AHSS

Steel	DP-340	DP-700	MS-1030	MS-1200
C (max %)	0.12	0.17	0.16	0.28
Si (max %)	0.4	0.4	0.4	0.4
Mn (max %)	1.6	1.7	1.8	1.3
P (max %)	0.025	0.02	0.02	0.02
S (max %)	0.01	0.01	0.01	0.01
Al (%)	$\geq$0.015	$\geq$0.01	0.015	0.015
Nb+Ti (max %)	0.1	0.15	0.1	0.1
Cr+Mo (max %)	1	1	1	1
V (max %)	0.2	-	-	-
B (max %)	0.005	0.005	0.005	0.01
Cu (max %)	0.2	0.2	0.2	0.2

2. Experimental study

2.1 Test materials and specimen

Specimens for the tensile coupon test were cut from four steel sheets and the basic information for the sheets are shown in Table 1, where DP is the abbreviation of dual phase and MS is the abbreviation of Martensitic. The sheets were labelled by their steel family and the nominal yield strength. Their typical chemical composition is shown in Table 2. All specimens were cut along the sheet rolling direction (i.e. specimens' longitudinal direction was parallel to sheet rolling direction).

The specimen dimension was designed per ASTM E8 [12], which was adopted by ASTM E21 [13] as shown in Figure 1. The actual thickness and width of each specimen was measured three times respectively at the center and two ends of the reduced parallel section, and the average of these three measurements were used for cross section area calculation. The coating of coated specimens made from DP-700 was removed by 1 Molar hydrochloric acid solution and the specimen thickness without coating were then measured. The coating thickness was calculated as around 0.04 mm for DP-700 specimens. The calculated cross section area was used for calculating stress during data processing.

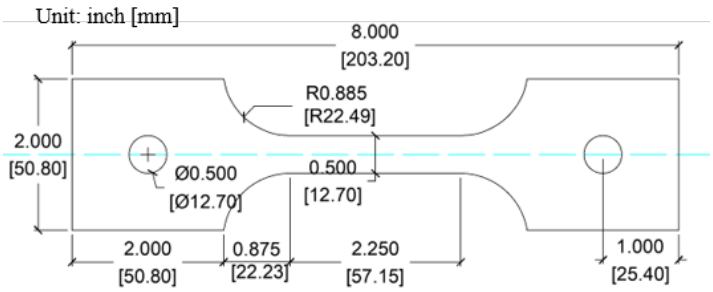

Figure 1: Design dimension of the tensile specimen

2.2 Testing equipment

The experiments were conducted in the Multi-Hazard Resilient Structures Lab at Johns Hopkins University. An MTS material loading system with an MTS model 661.21A-03 load cell was used for the tensile coupon tests. The capacity of the load cell is 89 kN (10 tons). The applied tension load on the specimen was directly output from the load cell. The strain measurement was conducted by an Epsilon model 3549 high temperature extensometer, which had a strain range of +20%/-10% and a temperature capacity of 1200°C.

An ATS 3210 series high temperature furnace with a capacity of 1150°C was used for heating process. The target temperature and heating rate in the furnace was controlled in three separate heating zones by an ATS temperature control system. Three internal K-type thermocouples were respectively placed in the center region of each heating zone to obtain the real-time temperature feedback. Additionally, three additional external K-type thermocouples were placed on the surface of the specimens at both ends and the center of the reduced parallel section and their readings were regarded as real-time temperature of the specimen.

2.3 Test procedure

For the steady-state test, the test procedure was designed per ASTM E21 [13]. The tensile specimen was first heated up to an elevated temperature and then loaded to fracture in a stabilized elevated temperature environment. During the heating process, the specimens experience thermal expansion, which would result in a compression force in the pinned specimens. The steady-state protocol dictates a heating phase at zero stress, therefore, during the heating stage the position of the pin was continuously adjusted to compensate for the thermal expansion. As the specimens are particularly vulnerable to buckling given their thin-walled geometry, and the force-control procedure has a non-infinite resolution and reaction time, a very small tension force (between 0 and 5 MPa) was maintained in the system throughout the heating.

Before the design of the test matrix, several trial tests were conducted. It was found that the yield strength at 700°C for the tested steels were 10% or lower of corresponding yield strength at ambient, which lead to a conclusion that testing at temperature above 700°C was unnecessary. Therefore, in this study, seven elevated temperature levels were set from ambient to 700°C. The heating rate was set to a constant of 10°C/min. When the elevated temperature was reached, an additional 15 min of heat conditioning at this target temperature was maintained to guarantee a uniformly distributed temperature throughout the specimen. Upon completion of the heat conditioning, tension load was applied to the specimen until fracture, while the temperature was kept constant at the specified target temperature. The loading rate was 0.762 mm/min during the loading process. The test matrix is shown in Table 3.

Table 3: Test matrix for steady-state tensile test

Steel	DP-340	DP-700	MS-1030	MS-1200
20°C	1	3	1	3
200°C	1	1	1	1
300°C	1	3	1	3
400°C	1	3	1	2
500°C	1	1	1	1
600°C	1	1	1	1
700°C	1	1	1	1

3. Discussions on the test results

3.1 Stress-strain curves

After the experiment, the readings from the high temperature extensometer was obtained as the engineering strain. The engineering stress was calculated as the applied load divided by the initial specimen cross section area. Therefore, for each steel at each elevated temperature, the engineering stress-strain relationship was obtained and the representatives are shown as the colorful solid lines in Figure 8, 9, 10 and 11.

For all four steels at all elevated temperatures, no obvious yield point is observed. Rather, the strain hardening process develops gradually. For DP-340 and DP-700, cases up to 400°C experience a longer straining hardening process to the ultimate strength; cases above 400°C reach the ultimate strength at lower strain level and experience a longer strain softening plateau until fracture. For MS-1030 and MS-1200, at 20°C and 200°C, specimens experience a longer strain hardening process to the ultimate strength; for cases above 200°C, specimens reach the ultimate strength at lower strain level and experience a longer strain softening until fracture; for cases at 300°C and 400°C, the strain softening is accomplished in a more rapid rate, while for cases at 500°C and above, the strain softening is slower and more stable.

For DP-340 and DP-700, their strengths are relatively stable

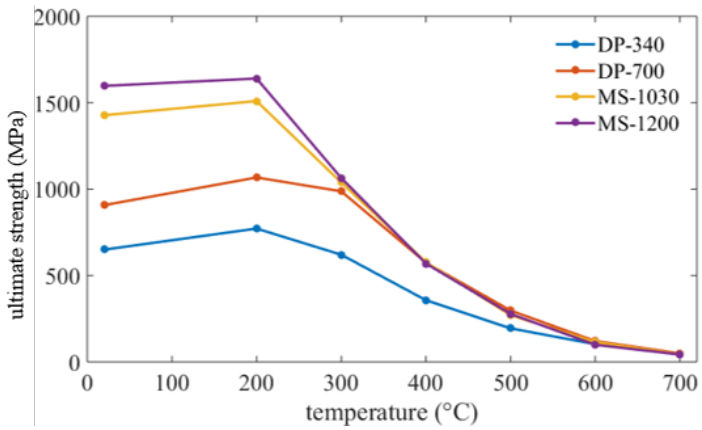

Figure 2: Ultimate strength at each elevated temperature

up to 300°C; even stronger strength than that at ambient is observed for 200°C and 300°C cases. When temperature reaches 400°C, the strength decreases in a rapid rate for each temperature increment. For MS-1030 and MS-1200, the strengths are relatively stable up to 200°C and then decreases rapidly for each temperature increment. The ultimate strength at each temperature is shown in Figure 2 to illustrate this tendency.

For DP-340 and DP-700, the elongation at fracture did not change significantly below 400°C but increased significantly at 500°C; then the elongation gradually decreased for higher temperature cases compared to 500°C case. For MS-1030 and MS-1200, the elongation at 200°C, 300°C and 400°C is close to each other, but obviously higher than the ambient case. The elongation reached its maximum at 500°C and then continuously decreased at 600°C and 700°C.

3.2 Material properties at elevated temperatures

The focus of this paper is the modeling of the stress-strain relationship of AHSS. Therefore, only the material properties required in existing or proposed stress-strain models are discussed in this section. Discussion in more detail on the test results is covered in another paper from the authors [14] focusing on the experiment prospective.

3.2.1 Elastic modulus

Generally speaking, the elastic modulus for a material was determined from the stress-strain curve as the slope of its initial linear elastic region. Unlike the type of steel with a clear yield point and yield plateau, for AHSS with gradual strain hardening process, it is less clear to define the linear elastic region. Huang and Young [15] provided a method to determine the slope of linear elastic region at ambient per ASTM standards and their method is shown in Equation 1. In this method, two points with stress equal to 20% and 45% of the nominal yield strength at ambient are used to calculate

Table 4: Elastic modulus at elevated temperature (in GPa)

Steel	DP-340	DP-700	MS-1030	MS-1200
20°C	230.0	183.3	215.6	204.5
200°C	167.5	173.8	219.1	165.5
300°C	132.7	192.2	177.5	161.3
400°C	152.3	169.5	157.1	127.9
500°C	105.6	96.6	64.5	65.6
600°C	88.5	66.4	43.1	38.0
700°C	87.4	40.3	22.5	21.2

the line slope between these two points, which is regarded as elastic modulus for the stress-strain curve. To adopt this method for cases at elevated temperature, an updated equation is proposed to include the steel strength deterioration results from elevated temperature environment as shown in Equation 2. The use of the ultimate strengths ratio in Equation 2 is needed because the nominal yield strength at elevated temperature T depends itself on the modulus, as detailed in the next section.

$$E_0 = \frac{\sigma_{n45} - \sigma_{n20}}{\varepsilon_{n45} - \varepsilon_{n20}} = \frac{0.45 \times \sigma_{yn0} - 0.20 \times \sigma_{yn0}}{\varepsilon_{n45} - \varepsilon_{n20}} = \frac{0.25 \times \sigma_{yn0}}{\varepsilon_{n45} - \varepsilon_{n20}} \quad (1)$$

where E_0 is the elastic modulus at ambient, σ_{n45} and ε_{n45} are the stress and strain of the point with 45% of the nominal yield strength, σ_{n20} and ε_{n20} are the stress and strain of the point with 20% of the nominal yield strength, and σ_{yn0} is the nominal yield strength at ambient.

$$E_T = \frac{0.25 \times \sigma_{ynT}}{\varepsilon_{n45T} - \varepsilon_{n20T}} = \frac{0.25 \times \sigma_{yn0}}{\varepsilon_{n45T} - \varepsilon_{n20T}} \times \frac{\sigma_{uT}}{\sigma_{u0}} \quad (2)$$

where E_T is the elastic modulus at elevated temperature T, σ_{ynT} is the nominal yield strength at elevated temperature T, ε_{n20T} and ε_{n45T} are the strains of the point with 20% and 45% of σ_{ynT}, and σ_{uT} and σ_{u0} are the ultimate strength at elevated temperature T and at ambient, respectively. By using this method, the elastic modulus is calculated as shown in Table 4.

3.2.2 Yield strength

Unlike material with a clear yield point, defining the yield point on a rounded stress-strain curve is more challenging. One commonly used method for the ambient case, after the determination of elastic modulus, is using the point at 0.2% proof stress (i.e. the point with a plastic strain of 0.002) as the yield point. The point is determined by the intersection of the experimental stress-strain curve and a line with a slope of elastic modulus E which passes through 0.002 on strain axis. However, due to the different performance of various materials (e.g. steels with highly rounded stress-strain curves) and the difficulty in calculating accurate elastic modulus at elevated temperature, this proof stress method might sometimes lead to unreasonable yield strength results. Therefore,

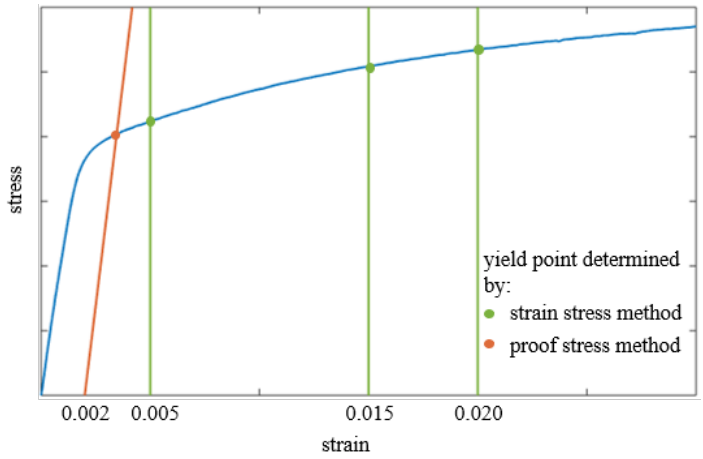

Figure 3: Illustration of yield point defined by strain stress method and proof stress method

Table 5: 0.2% proof stress at elevated temperature (in MPa)

Steel	DP-340	DP-700	MS-1030	MS-1200
20°C	409	677	1314	1381
200°C	433	713	1127	1178
300°C	361	671	886	845
400°C	274	474	500	486
500°C	173	256	224	217
600°C	97	110	94	78
700°C	42	42	25	29

some researchers also adopted total strain stress method. Point at total strain level of 0.5%, 1.5%, or 2.0% is used as the yield point, which has the advantage of being independent of the elastic modulus. The comparison between the two methods for determining the yield point is shown in Figure 3. For the standard side, American standards [1][2] do not provide clear definition; Eurocode 3: Part 1-2 [4] determines the yield strength by 2.0% strain stress; BS 5950 [3], although has been withdrawn, recommended stresses with all three total strain levels of 0.5%, 1.5% and 2.0% as yield strength; AS4100 [5] and Annex E of Eurocode 3: Part 1-2 [4] (which is designed for Class 4 steel and is applicable for this study) determine the yield strength by 0.2% proof stress. A summary of yield strength for steels at elevated temperature by 0.2% offset and 2.0% total strain methods, which are recommended by current standards, is shown in Table 5 and 6. To compare the difference of using these two methods, the ratio between yield strengths using the two methods for each material at each elevated temperature was calculated and illustrated in Figure 4. For DP-340 and DP-700, the difference is as large as around 20% up to 400°C and the difference decreases when the target temperature increases. For MS-1030 and MS-1200, the difference is around 10% at ambient and relatively stable at a level of 20% from 200°C to 700°C.

Table 6: 2.0% strain stress at elevated temperature (in MPa)

Steel	DP-340	DP-700	MS-1030	MS-1200
20°C	534	860	1419	1551
200°C	609	967	1440	1529
300°C	506	899	1032	1060
400°C	339	574	568	566
500°C	190	294	266	273
600°C	101	116	111	95
700°C	45	49	34	36

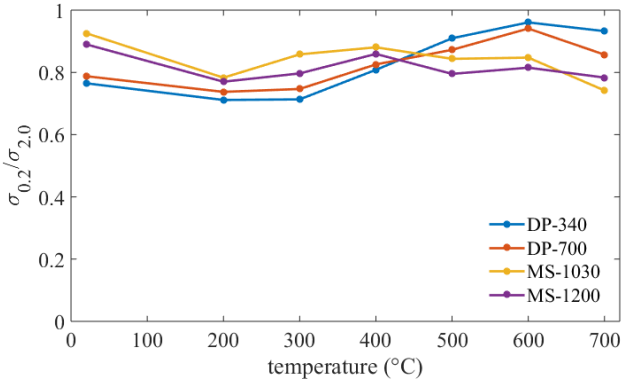

Figure 4: Comparison between yield strength using 0.2% proof stress and 2.0% total strain stress

4. Stress-strain model

Accurate modeling of stress-strain relationship is essential for the simulation of material performance in different conditions. Ramberg-Osgood (R-O) model [16] is the most commonly used method to describe rounded stress-strain relationship for metals including CFS. Previous research has been conducted on different types of steels for both ambient and high temperature cases by modifying the original R-O model. Two major types of transformation of the R-O model were proposed and adopted by researchers in the structural fire field. One transformation (referred as β model hereafter in this paper) [17][18] introduced a linear constant β to account for the characteristics of the stress-strain curve of the specific steels they studied and an exponential coefficient *n* to account for the effects resulting from high temperature. The expression of the model is shown Equation 3. Olawale [17] studied hot-rolled steel and selected a β of $\frac{3}{7}$ and Outinen [18] studied S355 steel and selected a β of $\frac{6}{7}$. In Lee's work [8], Equation 3 was adopted with an update, where *n* is set as a constant and β varies at each elevated temperature. The other transformation (referred as 2-stage model) [11] proposed a two-stage model for steels at elevated temperature based on the idea of two-stage models at ambient [19][20]. The model based on this idea is shown in Equations 4 for $\sigma_T \leq \sigma_{yT}$ and Equation 5 for $\sigma_{yT} \leq \sigma_T \leq \sigma_{uT}$. Because all transformations are based on the R-O model, in these updated models, stress is input and strain is output.

The models are designed to depict the stress-strain relationship up to the ultimate point; the strain softening after the ultimate point is not included.

$$\varepsilon_T = \frac{\sigma_T}{E_T} + \beta(\frac{\sigma_{yT}}{E_T})(\frac{\sigma_T}{\sigma_{yT}})^n \tag{3}$$

$$\varepsilon_T = \frac{\sigma_T}{E_T} + 0.002(\frac{\sigma_T}{\sigma_{yT}})^n \tag{4}$$

$$\varepsilon_T = \frac{\sigma_T - \sigma_{yT}}{E_{yT}} + \varepsilon_{uT}(\frac{\sigma_T - \sigma_{yT}}{\sigma_{uT} - \sigma_{yT}})^m + \varepsilon_{yT} \tag{5}$$

All aforementioned models were calibrated to the AHSS stress-strain curves from the experiments. Although these papers recommended values or predictive equations for β and/or the exponential coefficients based on test temperature, the recommendations were fitted from the specific steels they studied. By using their recommendations, poor fitting was obtained to AHSS tested here. Therefore, β and the exponential coefficients were recalibrated with AHSS stress-strain test curves using error minimization method to find the maximum R^2, which is calculated by Equation 6.

$$R^2 = 1 - \frac{SS_{res}}{SS_{tot}} = 1 - \frac{\sum_i(\varepsilon_{Ti} - \varepsilon_T(\sigma_{Ti}))^2}{\sum_i(\varepsilon_{Ti} - \bar{\varepsilon}_{Ti})^2} \tag{6}$$

where σ_{Ti} and ε_{Ti} are the stress and strain of data point i of the experimental curve at elevated temperature T; $\varepsilon_T(\sigma_{Ti})$ is the strain calculated by the model corresponding to σ_{Ti}; and $\bar{\varepsilon}_{Ti}$ is the average of experimental strains.

The stress-strain relationships for DP-700 and MS-1200 at 200°C (to represent cases below 400°C) and at 500°C (to represent cases equal or above 500°C) were used as examples to illustrate the best fitting using the two models as shown in Figure 5 and Figure 6. Including the examples, for DP-340 and DP-700 cases below 400°C, the 2-stage model provides accurate fitting for the first stage, while the fitting accuracy at the beginning and the end of the second stage is poor. For DP-340 and DP-700 cases at or above 500°C, the 2-stage model is able to provides accurate fitting up to around 90% of the ultimate strength, while the strain prediction is underestimated for the high stress range. The β model for all temperature range is able to provides a good fitting between the proportional limit and around 80% of the ultimate strength, while the remainder portions are poorly fitted.

A two-stage plus linear model for AHSS material at ambient was proposed by the authors [21], and it was updated in this paper to fit the cases at elevated temperature as shown in Figure 7. Similar to other models based on the R-O equation, the proposed model uses stress at elevated temperature as input and the output is the corresponding strain prediction. Due to this characteristic, the model describes the material behavior from origin to the ultimate point. The model is comprised of two stages plus a linear part. When $\sigma_T \leq \sigma_{pT}$,

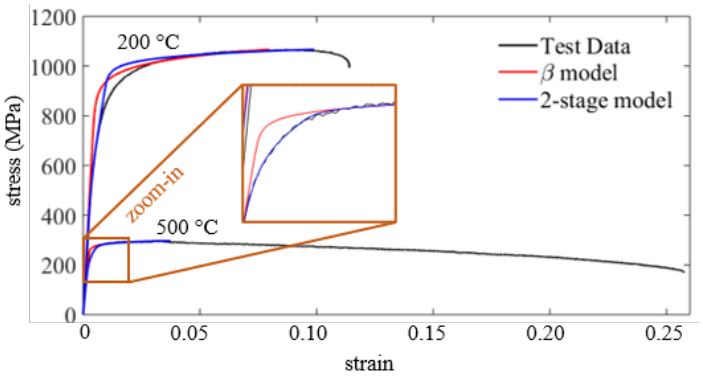

Figure 5: Optimal fitting examples for DP-700 using existing models

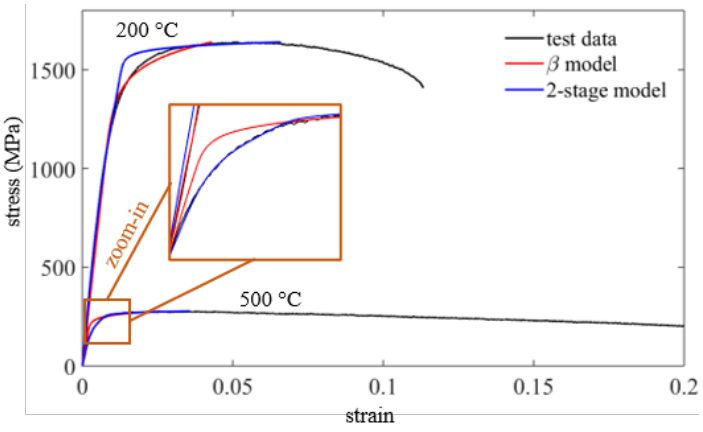

Figure 6: Optimal fitting examples for MS-1200 using existing models

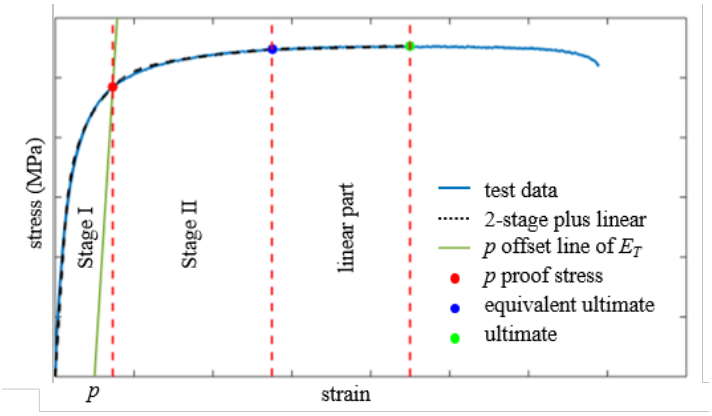

Figure 7: Schematic diagram for the proposed two-stage plus linear model

the first stage of the model is given by Equation 7. When $\sigma_{pT} < \sigma_T \leq \sigma_{euT}$, the second stage of the model is given by Equation 8. The final part is proposed as a line from the end of the second stage to the ultimate point.

$$\varepsilon_T = \frac{\sigma_T}{E_T} + p(\frac{\sigma_T}{\sigma_{pT}})^n \tag{7}$$

$$\varepsilon_T = \frac{\sigma_T - \sigma_{pT}}{E_{pT}} + (\varepsilon_{euT} - \varepsilon_{pT} - \frac{\sigma_{euT} - \sigma_{pT}}{E_{pT}})(\frac{\sigma_T - \sigma_{pT}}{\sigma_{euT} - \sigma_{pT}})^m + \varepsilon_{pT} \tag{8}$$

where p is the plastic strain of the demarcation point (with strain of ε_{pT} and stress of σ_{pT}) between the first and the second stage; E_{pT} is the tangent modulus at p proof stress and it is calculated by Equation 9. The demarcation point between the second stage and the final linear part is called the equivalent ultimate point. It has a stress of 99% of the ultimate strength and its strain and stress are ε_{euT} and σ_{euT} respectively. n and m are the exponential coefficients determining the model's degree of curvature for the first stage and the second stage respectively, and they are calculated by error minimization.

$$E_{pT} = \frac{E_T}{1 + pn\frac{E_T}{\sigma_{pT}}} \tag{9}$$

From the discussion in section 3.1, at different target temperature, the shape of the stress-strain curves have different characteristics. For DP-340 and DP-700, cases up to 400°C show a more rounded curve shape and the cases above 400°C show a sharper curve shape. This characteristic is also implied by the comparison between yield strength calculated by 0.2% proof stress and 2.0% strain stress in Figure 4. For MS-1030 and MS-1200, the ratio between 0.2% proof stress and 2.0% strain stress is relatively stable and close to 1. It has been concluded in the authors' previous work [21] that for rounded curves with higher degree of curvature (e.g. low temperature cases for DPs), using 0.2% proof stress as the demarcation point between the first and the second stage is not able to provide accurate fitting for DP-340 and DP-700; rather, using a proof stress with a higher plastic strain to define the demarcation point will increase the accuracy of the fitting. To find the proper offset for each AHSS at different elevated temperatures, models with different p, including 0.2%, 0.5%, 1.0%, 1.5% and 2.0%, were tested to find the optimal fitting by iterating the two exponential coefficients until the maximum R^2 between the test stress-strain data and the model data was found. It was found the recommended offset is affected by both material strength and the target temperature and a summary of the recommended offsets are shown in Table 7.

Table 7: Recommendation of offset p in percentage for proposed model based on material strength and test temperature

Steel	DP-340	DP-700	MS-1030	MS-1200
T<400°C	2.0%	1.0%	0.2%	0.2%
$T\geq$400°C	0.2%	0.2%	0.2%	0.2%

The optimal fittings using the proposed 2-stage plus linear model for AHSS at elevated temperatures are shown in Figures 8, 9, 10 and 11, which show excellent agreement between the test data and the proposed model. The test data is depicted by colorful solid lines and the corresponding model data is depicted by black dashed lines. From the discussion on the stress-strain relationships for different temperatures in Section 3.1, for DP-340 and DP-700, 400°C is the critical temperature that divided all cases into two groups below and above it. Temperature cases up to 400°C have more rounded curve shape while cases at or above 500°C have sharper curve shape. This observation is verified by the model fitting results choosing different offset point as the end of the first stage. For DPs, the offset selection was divided into two groups and the transition case was the 400°C case as shown in Table 7.

5. Conclusions

This paper presents a detailed numerical study on the stress-strain relationship at target elevated temperatures for two 1.4-mm thick DP steels and two 1.0-mm thick MS steels. The steady-state method was used and the test temperature ranged from ambient to 700°C. The stress-strain relationship for different steels vary in the tested temperature range. All four AHSS show a gradual strain hardening process and no well-defined yield point was observed. For steels with different strengths, the stress-strain curve for the lower strength steels (e.g. DP-340) has a larger degree of curvature compared to the higher strength steels (e.g. MS-1030 and MS-1200). For the same steel tested at different temperatures, the stress-strain curve for cases at lower tem-

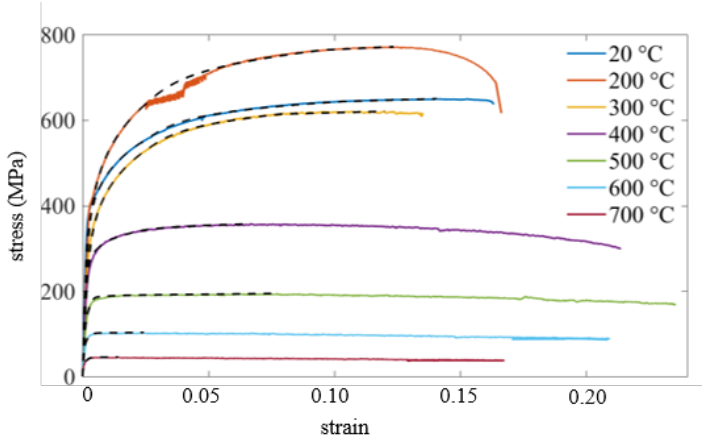

Figure 8: Comparison of stress–strain curves predicted using the proposed model with test results for DP-340

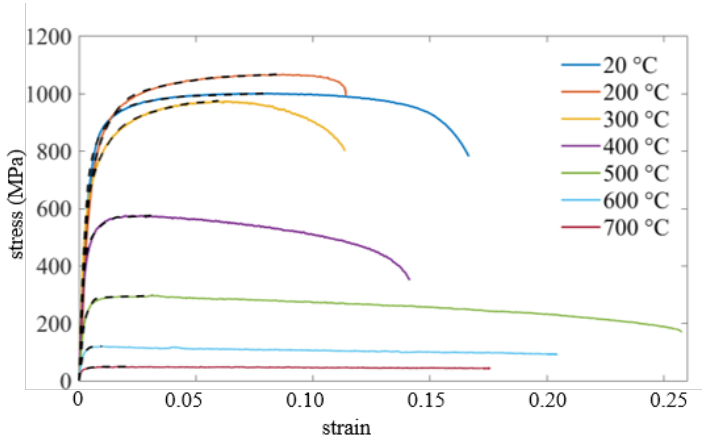

Figure 9: Comparison of stress–strain curves predicted using the proposed model with test results for DP-700

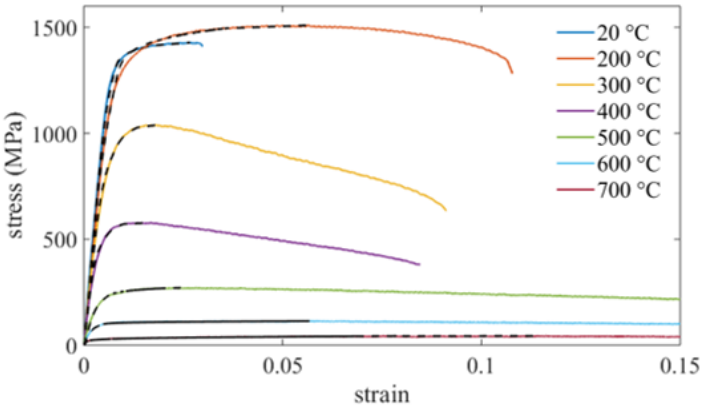

Figure 10: Comparison of stress–strain curves predicted using the proposed model with test results for MS-1030

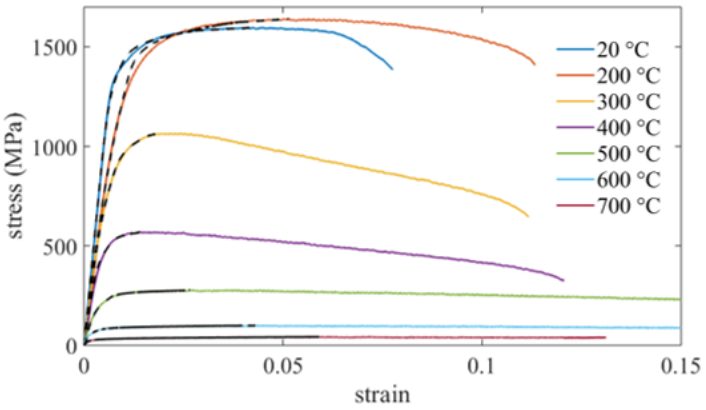

Figure 11: Comparison of stress–strain curves predicted using the proposed model with test results for MS-1200

perature has a more rounded shape; the stress-strain curve for cases with temperature at or higher than 500°C experience a longer strain softening plateau from ultimate point to fracture point. Two methods using the proof stress and total strain stress to define the yield point were discussed. For DP-340 and DP-700, the difference between the two methods is larger at lower test temperature due to the rounded shape of the stress-stain curve. For MS-1030 and MS-1200, the difference is relatively small and stable, which is generally within 20% for all tested temperatures. Existing models for the stress-strain relationship of steel at elevated temperature were discussed and they were recalibrated to fit AHSS test curves. However, none of them is able to provide accurate fittings. An updated two-stage plus linear model based on the Ramberg-Osgood equation is proposed to describe the stress-strain relationship of AHSS at elevated temperature. One clear benefit of the model, compared with some existing models, is its expressions are unified for all temperature cases. The method to define two critical points of the model were discussed. The fittings between the model built on parameters from the test and experimental AHSS stress-strain curves are excellent.

References

[1] AISC 360-16, “Specification for Structural Steel Buildings,” Chicago, IL, Tech. Rep., 2016.

[2] AISI S100-16, *North American Specification for the Design of Cold-Formed Steel Structural Members*. Washington, DC, U.S.A.: AISI, 2016.

[3] British Standards Institution, “BS 5950 Structural use of steelwork in building — part 8: code of practice for fire resistance design,” British Standards Institution (BSI), Tech. Rep., 2003.

[4] European Committee for Standardization (CEN), “Eurocode 3: Design of steel structures - Part 1-2: General rules - Structural fire design,” European Commit-

tee for Standardization (CEN), Brussels, Tech. Rep., 2005, pp. 1–81.

[5] Standards Australia, "AS 4100-1998 (R2016) Steel structures," Standards Australia, Sydney, Australia, Tech. Rep., 2016, pp. 1–238.

[6] T. Ranawaka and M. Mahendran, "Experimental study of the mechanical properties of light gauge cold-formed steels at elevated temperatures," *Fire Safety Journal*, vol. 44, no. 2, pp. 219–229, 2009, ISSN: 03797112. DOI: 10.1016/j.firesaf.2008.06.006.

[7] S. Keeler, M. Kimchi, and P. Mooney, *Advanced High-Strength Steels Application Guidelines*, 6.0. Brussels, Belgium: WorldAutoSteel, 2017. [Online]. Available: https://www.worldautosteel.org/projects/advanced-high-strength-steel-application-guidelines/.

[8] J. H. Lee, M. Mahendran, and P. Makelainen, "Prediction of mechanical properties of light gauge steels at elevated temperatures," *Journal of Constructional Steel Research*, vol. 59, no. 12, pp. 1517–1532, Dec. 2003, ISSN: 0143974X. DOI: 10.1016/S0143-974X(03)00087-7.

[9] W. Chen and J. Ye, "Mechanical properties of G550 cold-formed steel under transient and steady state conditions," *Journal of Constructional Steel Research*, vol. 73, pp. 1–11, 2012, ISSN: 0143974X. DOI: 10.1016/j.jcsr.2011.12.010. [Online]. Available: http://dx.doi.org/10.1016/j.jcsr.2011.12.010.

[10] Y. Huang and B. Young, "Stress-strain relationship of cold-formed lean duplex stainless steel at elevated temperatures," *Journal of Constructional Steel Research*, vol. 92, pp. 103–113, 2014, ISSN: 0143974X. DOI: 10.1016/j.jcsr.2013.09.007. [Online]. Available: http://dx.doi.org/10.1016/j.jcsr.2013.09.007.

[11] J. Chen and B. Young, "Stress-strain curves for stainless steel at elevated temperatures," *Engineering Structures*, vol. 28, no. 2, pp. 229–239, 2006, ISSN: 01410296. DOI: 10.1016/j.engstruct.2005.07.005.

[12] ASTM E8, "Standard Test Methods for Tension Testing of Metallic Materials," ASTM International, West Conshohocken, PA, Tech. Rep. 13a, 2016, pp. 1–27. DOI: 10.1520/E0008.

[13] ASTM E21, "Standard Test Methods for Elevated Temperature Tension Tests of Metallic Materials," ASTM International, West Conshohocken, PA, Tech. Rep., 2017, pp. 1–8.

[14] X. Yan, Y. Xia, H. B. Blum, and T. Gernay, "Elevated temperature material properties of advanced high strength steel alloys," *Journal of Constructional Steel Research*, vol. 174, p. 106 299, Nov. 2020, ISSN: 0143974X. DOI: 10.1016/j.jcsr.2020.106299.

[15] Y. Huang and B. Young, "The art of coupon tests," *Journal of Constructional Steel Research*, vol. 96, pp. 159–175, May 2014, ISSN: 0143974X. DOI: 10.1016/j.jcsr.2014.01.010. [Online]. Available: https://linkinghub.elsevier.com/retrieve/pii/S0143974X14000212.

[16] W. Ramberg and W. R. Osgood, "Description of stress-strain curves by three parameters," *National Advisory Committee For Aeronautics*, no. I, Technical Note No. 902, 1943. [Online]. Available: http://hdl.handle.net/2060/19930081614.

[17] A. O. Olawale and R. J. Plank, "The collapse analysis of steel columns in fire using a finite strip method," *International Journal for Numerical Methods in Engineering*, vol. 26, no. 12, pp. 2755–2764, Dec. 1988, ISSN: 0029-5981. DOI: 10.1002/nme.1620261212. [Online]. Available: http://doi.wiley.com/10.1002/nme.1620261212.

[18] J. Outinen, "Mechanical properties of structural steels at elevated temperatures," PhD thesis, Helsinki University of Technology, Finland, 1999.

[19] E. Mirambell and E. Real, "On the calculation of deflections in structural stainless steel beams: An experimental and numerical investigation," *Journal of Constructional Steel Research*, vol. 54, no. 1, pp. 109–133, Apr. 2000, ISSN: 0143-974X. DOI: 10.1016/S0143-974X(99)00051-6.

[20] K. J. Rasmussen, "Full-range stress-strain curves for stainless steel alloys," *Journal of Constructional Steel Research*, vol. 59, no. 1, pp. 47–61, Jan. 2003, ISSN: 0143974X. DOI: 10.1016/S0143-974X(02)00018-4.

[21] Y. Xia, Z. Li, B. Schafer, and H. Blum, "Material property characterization of advanced high strength cold-formed steel," in *Advances in Engineering Materials, Structures and Systems: Innovations, Mechanics and Applications*, 2019, pp. 1083–1088, ISBN: 9781138386969. DOI: 10.1201/9780429426506-188.